

## Article

# Effects of Inorganic Minerals and Kerogen on the Adsorption of Crude Oil in Shale

Yanyan Zhang , Shuifu Li <sup>\*</sup>, Shouzhi Hu and Changran Zhou

School of Earth Resources, China University of Geosciences (Wuhan), Wuhan 430074, China

<sup>\*</sup> Correspondence: lishf@cug.edu.cn

**Abstract:** Shale oil stored in the shale system occurs mainly in adsorbed and free states, and ascertaining the amount of adsorbed crude oil in shale is a method of ascertaining its free oil content, which determines the accuracy of shale oil resource evaluation. Both inorganic minerals and kerogen have the ability to adsorb crude oil, but there is controversy surrounding which plays the greatest part in doing so; clarifying this would be of great significance to shale oil resource evaluation. Therefore, in this study, the evolution states of inorganic minerals and kerogen in shale were changed using pyrolysis, and the adsorbents were prepared for crude oil adsorption experiments, to explore the effects of inorganic minerals and kerogen on the crude oil adsorption of shale. The results showed that the differences in kerogen's structural units and content in organic-rich shale (TOC = 1.60–4.52%) had no obvious effects on its crude oil adsorption properties. On the contrary, inorganic minerals, as the main body of shale, played a dominant role in the adsorption of crude oil. The composition and evolution of the inorganic minerals controlled the surface properties of shale adsorbents, which is the main reason for the different crude oil adsorption properties of the different types of adsorbents. The results of this study are helpful in improving our understanding of the performance and mechanisms of shale in adsorbing crude oil and promoting the development of shale oil resource evaluation.

**Keywords:** oil; adsorption experiment; inorganic minerals; kerogen; thermal simulation of adsorption



**Citation:** Zhang, Y.; Li, S.; Hu, S.; Zhou, C. Effects of Inorganic Minerals and Kerogen on the Adsorption of Crude Oil in Shale. *Energies* **2023**, *16*, 2386. <https://doi.org/10.3390/en16052386>

Academic Editors: Reza Rezaee, Shu Tao and Dameng Liu

Received: 15 January 2023

Revised: 12 February 2023

Accepted: 27 February 2023

Published: 2 March 2023



**Copyright:** © 2023 by the authors. Licensee MDPI, Basel, Switzerland. This article is an open access article distributed under the terms and conditions of the Creative Commons Attribution (CC BY) license (<https://creativecommons.org/licenses/by/4.0/>).

## 1. Introduction

Shale oil is a liquid petroleum resource that is retained and enriched in the shale system after hydrocarbon generation and expulsion from source rocks, and it will be an essential replacement resource in the future. Shale oil stored in the shale system occurs mainly in its free and adsorption states; because the former is the main contributor to productivity, the accurate evaluation of free shale oil content is an important prerequisite to shale oil exploration and development [1,2]. However, there is usually some deviation in the results upon directly quantifying the free oil content, so the indirect calculation of free oil content through adsorbed and total oil content is attracting increasing attention [3–6]. Previous studies indicated that the liquid hydrocarbon adsorption properties of kerogen per unit mass are much higher than those of inorganic minerals; thus, previous studies mainly considered the adsorption of total organic carbon (TOC) on liquid hydrocarbons [7–11], among which the most intuitive and widely accepted method for evaluating the potential producibility of shale oil is the oil saturation index (OSI) ( $S_1/TOC$ ) [1,10–13]. However, when evaluating the potential of continental shale oil resources in some areas of China, the results of OSI do not precisely match the actual exploration results, which indicates that it is not sufficient to consider only the adsorption of liquid hydrocarbons on organic carbon [4,14,15].

Actually, the inorganic minerals (such as clay, quartz, feldspar, pyrite, carbonate, etc.) in shale still have a certain effect on the adsorption of liquid hydrocarbon [16–18]. Despite the adsorption properties of organic matter being much higher than those of inorganic minerals, with inorganic minerals forming the main part of shale, their relative content is

much higher than the content of kerogen; so, the liquid hydrocarbon adsorption capacity of inorganic minerals cannot be ignored [19–21]. Meanwhile, the changes in the pore characteristics and surface properties of shale will affect its hydrocarbon adsorption properties because of the process of sedimentation and the evolution of inorganic minerals and kerogen in shale [22–24]; thus resulting in the capacity of shale to adsorb liquid hydrocarbons not being equivalent to summing the capacity of purified kerogen and different types of purified inorganic minerals to adsorb liquid hydrocarbons [21,25]. Therefore, to research the overall crude oil adsorption capacity of organic-rich shale, the adsorption properties of inorganic minerals and kerogen must be considered simultaneously. At present, there are many reports of different types and maturities of purified kerogen adsorbing pure hydrocarbon liquids [9,26,27], and the purified inorganic mineral (or mixed purified inorganic mineral) adsorption of liquid hydrocarbons has also been explored [17,28,29]. However, at present, the results of these studies cannot completely or effectively guide the exploration of shale oil [25,30]. Therefore, using actual shale as an adsorbent and actual crude oil as an adsorbate in crude oil adsorption experiments may have more practical significance and facilitate guidance.

In order to clarify the influence of kerogen's structural and inorganic mineral composition and evolution in shale on its crude oil adsorption properties, this experiment used actual shale and crude oil from the same region. Under the condition of inorganic minerals and kerogen existing simultaneously, the shale samples underwent pyrolysis, and extracts were prepared of the shale adsorbents that contained different kerogen content and structures and different transformation degrees of inorganic minerals. After performing the crude oil adsorption experiments, according to the organic carbon content and the composition characteristics of inorganic minerals in the shale adsorbents, we analyzed the effects of inorganic minerals and kerogen on crude oil adsorption in shale.

## 2. Samples

The shale samples were collected from the Cheng 2 well in the central deep sag area of the Biyang Depression. A total of five shale samples (①~⑤ in Figure 1) were selected from the fifth shale layer of the third member of the Hetaoyuan formation ( $Eh_3$ ), at a vertical depth of 2771–2797 m. This depression is a secondary structural unit of the Nanxiang Basin, located in Tanghe County and Biyang County, Henan Province, China. Covering an area of about 1000 km<sup>2</sup>, it is a Meso-Cenozoic (Cretaceous–Paleogene–Neogene) rift depression [31]. According to the structure, the depression can be further divided into three subunits, including the northern slope belt, central deep sag, and southern steep slope belt. The central deep sag sedimented the thickness strata of the Paleogene (which is the main enrichment area for lithologic and shale oil reservoirs [32]), includes the Dacangfang, Yuhuangding, Hetaoyuan ( $Eh_1$ ,  $Eh_2$ ,  $Eh_3$ ) and Liaozhuang formations from the bottom to the top. Moreover, the third member of the Hetaoyuan formation ( $Eh_3$ ) can be divided into eight sand formations ( $Eh_3^I \sim Eh_3^{VIII}$ ). There are six layers of organic-rich shale developed in  $Eh_3^{III} \sim Eh_3^{VI}$  in the central deep depression [5,33]. Based on wireline logs and core sampling analysis (Rock-Eval, GC-MS, etc.), the fifth shale layer was the thickest and most widely distributed, was abundant in retained hydrocarbons, and was the main target layer of shale oil exploration in this area [5,32].

Previous studies have shown that the third member of the Hetaoyuan formation ( $Eh_3$ ) in the deep sag of the Biyang Depression is mainly composed of dark-gray and gray shale interbedded with dolomite and sandstone [32]. The types of kerogen are mainly type I and type II<sub>1</sub>, with little type II<sub>2</sub> [34]. The maturity of organic matter is at the low stage ( $Ro\% \approx 0.7\%$ ; average  $T_{max} \approx 446.35$  °C) [5]. The crude oil samples used in the adsorption experiment were from the same layer in the same area, and the characteristics of the crude oil group were as follows: saturated hydrocarbon (Sat.): 60.7 wt%, aromatic hydrocarbon (Aro.): 13.5 wt%, non-hydrocarbon and asphaltene (Res. + Asp.): 25.7 wt%; this is normal crude oil.

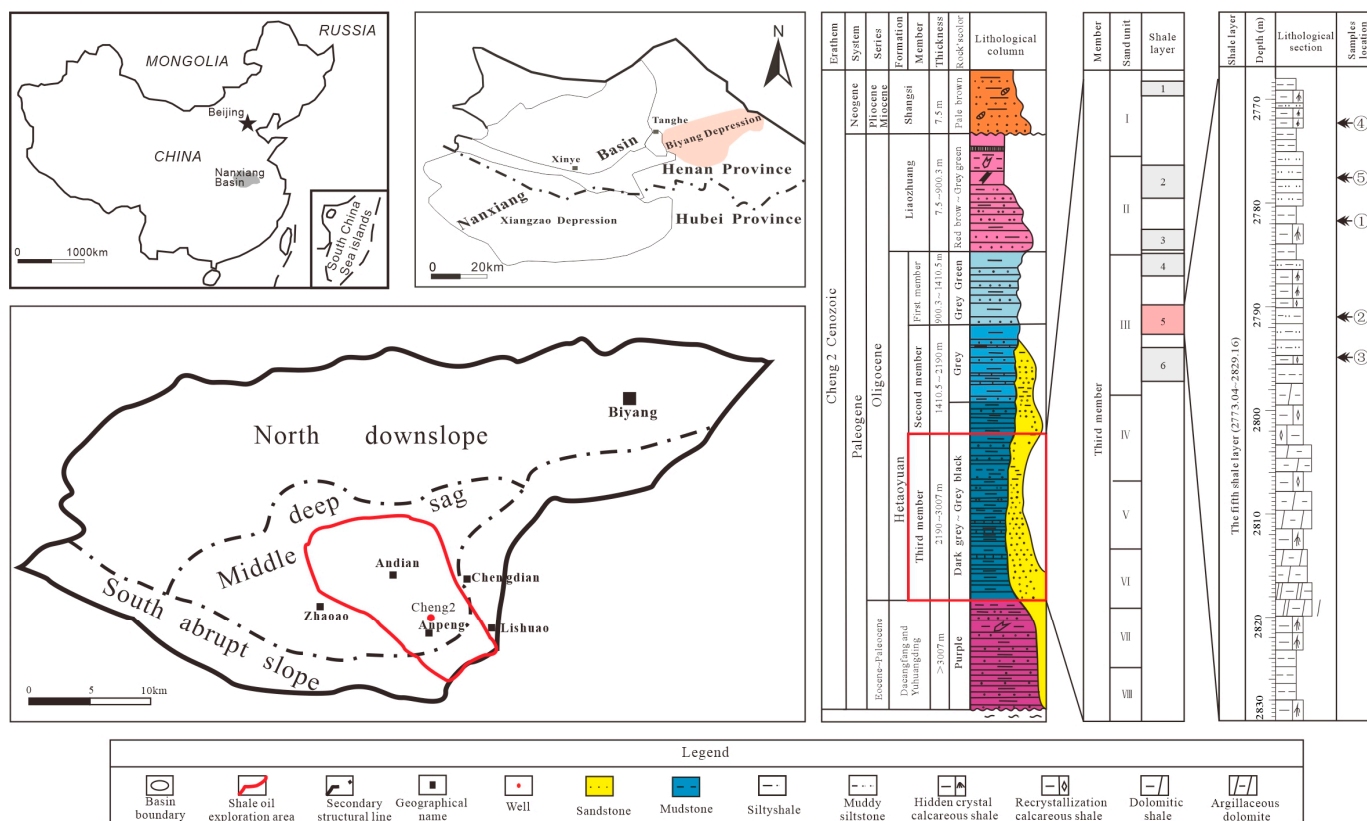


**Figure 1.** Location and generalized stratigraphic columns of the Biyang Depression and sample locations (Adapted with permission from Ref. [5]. 2016, Elsevier, adapted with permission from Ref. [33]. 2019, Elsevier).

### 3. Methodology

#### 3.1. Preparation of Adsorbents

Organic carbon in shale includes insoluble kerogen and soluble asphaltene. Kerogen is the organic adsorptive carrier (adsorbent) for soluble asphaltene, and soluble asphaltene is the adsorbed object (adsorbate); so, it is more scientific to determine the amount of oil adsorbed by kerogen than by total organic matter [27,35,36]. According to the principle of the hydrocarbon generation of kerogen and the theory of the kerogen structure model [37], in the process of hydrocarbon generation, part of the reactive kerogen can be directly converted into oil and gas (this is called effective carbon); meanwhile, the other part, despite participating in the process of hydrocarbon generation, is not converted into hydrocarbon but into residual carbon (RC). However, the inert kerogen neither participates nor is affected by hydrocarbon generation, so it can be called dead carbon (in this paper, the residual carbon and dead carbon are collectively called ineffective carbon, dividing the organic carbon in kerogen into two parts: effective carbon and ineffective carbon) [10,38]. Because reactive kerogen and inert kerogen represent a theoretical model, we could not obtain separate kerogen with these structural units, but we could measure the effective carbon (TOC > RC) and ineffective carbon (TOC ≈ RC) in kerogen via pyrolysis to measure the reactivity and inertia of kerogen. In this way, we could explore the oil adsorption properties of different kerogen structural units for crude oil.

Before preparing the adsorbents, the carbonate minerals in shale needed to be removed using hydrochloric acid (HCl). The main reason for this was that the upper layer of Eh<sub>3</sub> in the Biyang Depression was formed in an alkaline environment, which limited the dissolution of carbonate minerals in the early period of diagenesis and resulted in the precipitation and cementation of carbonate minerals in the late period of diagenesis [39]. However, during the process of preparing the adsorbents via thermal treatment, carbonate

minerals tended to decompose after 650 °C. This will lead to a significant increase in the specific surface area (SSA) of the samples, and the CO<sub>2</sub> generated will affect the measurement of TOC [40–42]. The former will seriously affect the adsorption performance of shale adsorbents [19,21,25,29], while the latter will affect the evaluation of kerogen's adsorption properties in shale adsorbents. Therefore, in order to keep the inorganic mineral composition of shale adsorbents obtained via pyrolysis treatment as consistent as possible, it was necessary to remove carbonate minerals in shale via hydrochloric acid treatment before pyrolysis treatment of the shale samples.

The temperature conditions for preparing the adsorbents were those of the Rock-Eval analysis method. A shale sample treated with hydrochloric acid (abbreviated as T<sub>HCl</sub>) was heated in a N<sub>2</sub> flow at 300 °C for 1 h to remove the pyrolytic hydrocarbon S<sub>1</sub>. Then, on the pyrolysis products, we used DCM (dichloromethane) and MeOH (methanol) (93:7, v/v) for extraction for 72 h; after that, extraction was conducted for 72 h using methanol, acetone, and benzene (MAB) (2:5:5, v/v/v) to remove as much of the soluble organic matter in the pyrolysis products of shale as possible. After finishing the above process, the Type-A (abbreviated as T<sub>A</sub>) adsorbent that contained the effectiveness of carbon in kerogen (containing available carbon+ and ineffective carbon+ inorganic minerals) was prepared. To prepare the Type-B adsorbent (abbreviated as T<sub>B</sub>) that contained the carbon in kerogen ineffective (containing ineffective carbon+ inorganic minerals), a fresh shale sample of T<sub>HCl</sub> was heated in a N<sub>2</sub> flow at 650 °C for 1 h to remove the pyrolytic hydrocarbons S<sub>1</sub> and S<sub>2</sub>; then, we treated the pyrolysis products with the same extraction process as the extract for T<sub>A</sub>, removing as much of the soluble organic matter as possible. To prepare the Type-C (represented by T<sub>C</sub>) adsorbent that removed kerogen (containing only inorganic minerals), a fresh shale sample of T<sub>HCl</sub> was heated in an O<sub>2</sub> flow at 900 °C for 1 h to remove all organic carbon; then, we treated the pyrolysis products with the same extraction process as the extract for T<sub>A</sub>, removing the soluble organic matter. The adsorbents and T<sub>HCl</sub> were subsequently analyzed using XRD and Rock-Eval to verify the quality.

X-ray diffraction (XRD) analysis of the adsorbents was performed using a German Bruker AXS D8 Advance, with a Cu target; a ceramic X-ray tube; operation at 40 kV and 40 mA; a focal spot size of 0.4 × 12 mm; a LynxEye XE detector; test mode: wide angle of 5°–90°; and a rate of 5°/min. XRD analysis was completed in the Analysis and Test Center of the School of Materials and Chemistry, China University of Geosciences (Wuhan).

Rock-Eval analysis of the adsorbents was performed according to Lafargue et al. (1998) [6]. The powder samples (20 g and about 80 mesh, ≤178 μm in grain size) were analyzed using Rock-Eval 6 (manufactured by Vinci Technologies in France). Rock-Eval analysis and data processing were performed by the Guangzhou Institute of Geochemistry, Chinese Academy of Sciences (GIG, Guangzhou, China). Subsequently, we obtained the pyrolysis data of S<sub>1</sub>, S<sub>2</sub>, total organic carbon (TOC), residual organic carbon (RC), mineral carbon (MinC), T<sub>max</sub> (°C), and the hydrogen index (HI) of the adsorbents.

### 3.2. Adsorption Experimental Method

Generally, an adsorbate solution with a low or high concentration can reach adsorption equilibrium with the adsorbent within a certain period of time (many liquid adsorption experiments measure the concentration of the adsorbate solution in the adsorption equilibrium stage by spectrophotometry to estimate the adsorption capacity of the adsorbent [17,43]. Therefore, there is still fluidity of the unadsorbed adsorbate molecules in the adsorbate solution at the adsorption equilibrium state); when the concentration of adsorbate reaches a certain level at which the adsorbent reaches saturated adsorption equilibrium, the adsorbent will no longer receive adsorbate. Even if the concentration of the adsorbate increases further, it will not affect the adsorption capacity of the adsorbent [21,28]. In other words, the crude oil (adsorbate) in the formation fluid (such as the oil–water solution containing salt and other soluble substances), under geological conditions, does not need to satisfy saturated adsorption by inorganic minerals and kerogen (adsorbents). After the crude oil in the formation fluid and the inorganic minerals and kerogen reach

adsorption equilibrium, the unadsorbed crude oil still has mobility. This principle is often used to reduce the adsorption equilibrium concentration of crude oil and improve its mobility by injecting hot water, gas, and other polymer solutions to enhance oil recovery (EOR) in the secondary and tertiary oil recovery stages of the oilfield [44,45]. Therefore, the setting of the adsorbate content (crude oil) in the experiment should be close to the content of chloroform bitumen A in geological samples. At the same time, in many studies on the organic matter adsorption properties of inorganic minerals, most choose single or mixed standard samples as adsorbates or adsorbents [17,20,46,47]. However, when crude oil is adsorbing on shale, different types of compounds and multifunctional carbon compounds in crude oil compete for the chemical bonds of the adsorbent for adsorption, so using crude oil as an adsorbate could more effectively reflect practical geological problems.

Ertas et al. [8] tested kerogen swelling under high-pressure and closed conditions, and found that the average swelling ratio at 150 °C was slightly higher than that at 30 °C and 90 °C, indicating that temperature affects kerogen swelling [26]. Therefore, the simulated temperature of this adsorption experiment was set at 90 °C, which was close to the actual formation temperature of the sample. Pernyeszi et al. conducted the adsorption of asphaltenes on clay and reservoir rocks by shaking them at 298 K for 24 h, and adsorption equilibrium was reached after the reaction [17]. Daughney [28] reported that adsorption equilibration was achieved within 24 h for the sorption of oil onto powdered quartz in both the presence and absence of an aqueous phase. Ertas et al. (2006) also verified that an adsorbate solution could reach adsorption equilibrium within 24 h at 30 °C, 90 °C, and 150 °C [8]. In fact, in many reports, it was found that the adsorption equilibrium time of organic matter on inorganic minerals only took tens to hundreds of minutes [43,48,49]. Furthermore, previous studies have shown that an increase in temperature reduced the time taken to reach adsorption equilibrium [50,51]. Therefore, because the simulated temperature of this experiment was close to the temperature of the formation where the shale sample was located (90 °C), combined with the above experience, continuing the experiment at 90 °C for 24 h was enough to reach adsorption equilibrium.

The conditions for each adsorption experiment are shown in Table 1. To ensure the adsorbate was evenly distributed in the adsorbents, it was necessary to dilute the crude oil with DCM and fully mix it with the adsorbent in the lining of the autoclave (25 mL), and then, wait for the DCM to evaporate completely. The adsorption experiment continued at 90 °C for 24 h, and then, the unadsorbed hydrocarbons were recovered via extraction.

**Table 1.** Conditions used in the adsorption experiments.

Sample No.	Chloroform Bitumen C (wt.%)	Temperature of Adsorbent Preparation (°C)	Adsorbent No.	Weight of Adsorbent/Adsorbate (g)		
				Adsorbent Content	Calculate Adsorbate Content	Adsorbate Content
1	0.597	300	1-T <sub>A</sub>	10.0534	0.0601	0.0603
		650	1-T <sub>B</sub>	10.0457	0.0600	0.0601
		900	1-T <sub>C</sub>	10.0285	0.0599	0.0600
2	0.589	300	2-T <sub>A</sub>	10.1000	0.0595	0.0591
		650	2-T <sub>B</sub>	10.3014	0.0607	0.0606
		900	2-T <sub>C</sub>	10.3354	0.0609	0.0606
3	0.479	300	3-T <sub>A</sub>	10.0139	0.0480	0.0478
		650	3-T <sub>B</sub>	10.2368	0.0490	0.0490
		900	3-T <sub>C</sub>	10.3310	0.0495	0.0498

Table 1. Cont.

Sample No.	Chloroform Bitumen C (wt.%)	Temperature of Adsorbent Preparation (°C)	Adsorbent No.	Weight of Adsorbent/Adsorbate (g)		
				Adsorbent Content	Calculate Adsorbate Content	Adsorbate Content
4	0.986	300	4-T <sub>A</sub>	9.6927	0.0956	0.0989
		650	4-T <sub>B</sub>	10.0054	0.0987	0.0975
		900	4-T <sub>C</sub>	10.0219	0.0988	0.0989
5	0.575	300	5-T <sub>A</sub>	9.9344	0.0571	0.0574
		650	5-T <sub>B</sub>	10.1426	0.0583	0.0582
		900	5-T <sub>C</sub>	10.3579	0.0596	0.0601

Here, in Table 1, 1-T<sub>A</sub> represents the Type-A adsorbent of sample 1 that was treated with hydrochloric acid to remove the pyrolytic hydrocarbon S<sub>1</sub> (heated in a N<sub>2</sub> flow at 300 °C for 1 h) and the soluble organic matter; 1-T<sub>B</sub> represents the Type-B adsorbent of sample 1 that was treated with hydrochloric acid to remove the pyrolytic hydrocarbons S<sub>1</sub> and S<sub>2</sub>, (heated in a N<sub>2</sub> flow at 650 °C for 1 h) and the soluble organic matter; 1-T<sub>C</sub> represents the Type-C adsorbent of sample 1 that was treated with hydrochloric acid to remove all of the organic matter (heated in an O<sub>2</sub> flow at 900 °C for 1 h). Furthermore, 2-T<sub>A</sub>, 2-T<sub>B</sub> and 2-T<sub>C</sub> represent shale adsorbents prepared by the same thermal decomposition and extraction process as 1-T<sub>A</sub>, 1-T<sub>B</sub> and 1-T<sub>C</sub>, respectively, for shale powder samples after hydrochloric acid treatment. The other adsorbent codes also represent the corresponding treatment procedures for the corresponding samples.

## 4. Results

### 4.1. Adsorbent Properties

The quality of the adsorbent is the key to a successful adsorption experiment; so, it was necessary to test the quality of the adsorbent before the adsorption experiment. For the detection of adsorbent properties, we mainly used XRD analysis to detect the composition and content of inorganic minerals, and Rock-Eval analysis to detect various indicators of organic matter.

T<sub>HCl</sub> and the adsorbents of T<sub>A</sub> (heated in a N<sub>2</sub> flow at 300 °C), T<sub>B</sub> (heated in a N<sub>2</sub> flow at 650 °C), and T<sub>C</sub> (heated in an O<sub>2</sub> flow at 900 °C) were analyzed via XRD (Figure 2), and the relative contents of the main inorganic minerals were statistically analyzed (Figure 3). The result showed that T<sub>HCl</sub> and the adsorbents mainly contained quartz (Q), orthoclase (Or), plagioclase (Pl), illite (I), illite/smectite (I/S), and a little chlorite (Ch), among which quartz had the highest relative content. Pyrolysis treatment under different conditions had a great influence on the composition and content of inorganic minerals in shale.

With the increased temperature in the adsorbent preparation, the illite diffraction peak intensity increased significantly (Figure 2), which was due to the transformation of illite/smectite to illite [52–54]. At the same time, the diffraction peak intensity of plagioclase also increased. This was due to the consumption of K<sup>+</sup> in the transformation of illite/smectite to illite; as long as the conversion exists, the dissolution of orthoclase will continue until exhausted [55]. Moreover, plagioclase will be difficult to dissolve, even when precipitated, because of the buffering of Na<sup>+</sup> produced by the transformation of illite/smectite to illite [55,56]. Subsequently, when the temperature of the adsorbent preparation reaches about 650 °C, the illite/smectite is completely transformed, and the plagioclase gradually decomposes and its diffraction peak intensity is reduced [57]. Meanwhile, the dehydroxylation reaction of illite will also reduce its diffraction peak intensity. When the temperature of the adsorbent preparation reaches about 900 °C, the diffraction peak intensity of illite decreases further due to the high degree of the dehydroxylation reaction and a certain degree of amorphous transformation (sintering phenomenon) [58–63].



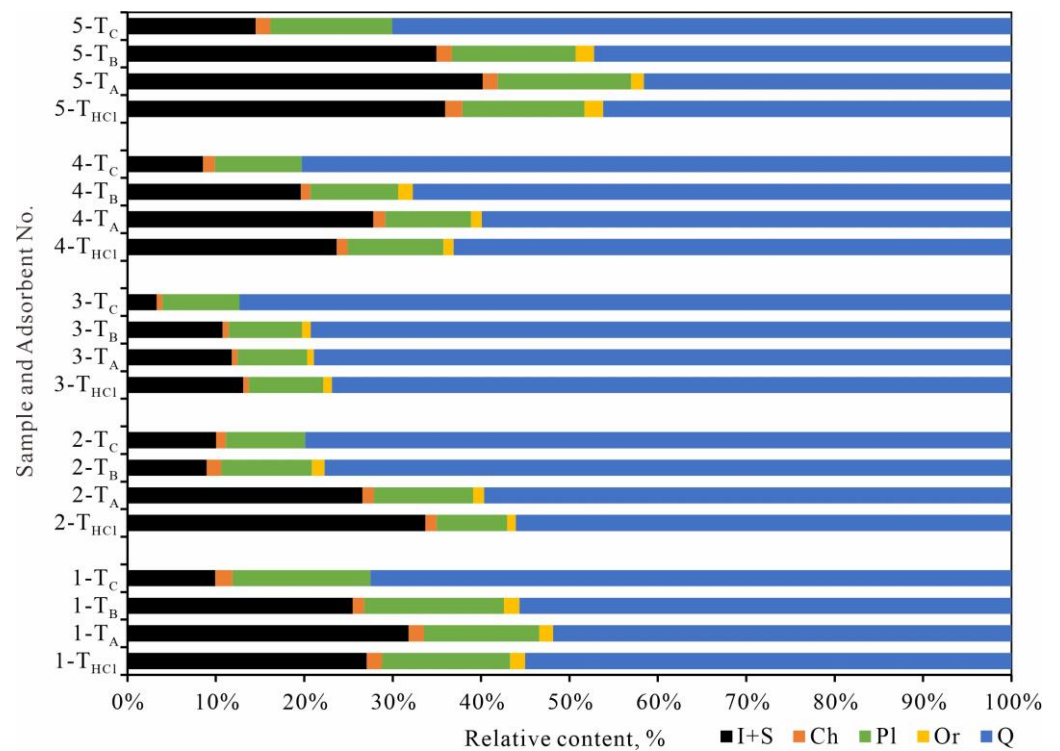


**Figure 3.** Relative contents of main inorganic minerals in T<sub>HCl</sub> and adsorbents. I + S: illite + smectite + illite/smectite.

**Table 2.** Rock-Eval analysis data of T<sub>HCl</sub> and adsorbents.

No.	S <sub>1</sub> (mg/g)	S <sub>2</sub> (mg/g)	TOC (wt.%)	RC (wt.%)	MinC (wt.%)	Tmax (°C)	HI (mg/g)
1-T <sub>HCl</sub>	2.58	21.18	4.81	2.83	0.15	446	440
1-T <sub>A</sub>	0.04	18.44	4.49	2.94	0.15	445	411
1-T <sub>B</sub>	0.01	0	3.29	3.28	0.07	486	0
1-T <sub>C</sub>	0	0	0	0	0	486	0
2-T <sub>HCl</sub>	0.06	6.55	2.41	1.84	0.16	440	272
2-T <sub>A</sub>	0.08	4.45	2.03	1.64	0.09	440	219
2-T <sub>B</sub>	0.06	0.01	1.76	1.75	0.12	297	1
2-T <sub>C</sub>	0	0	0.01	0.01	0.01	399	0
3-T <sub>HCl</sub>	0.26	22.42	4.82	2.92	0.07	444	465
3-T <sub>A</sub>	0.04	20.44	4.52	2.8	0.14	445	452
3-T <sub>B</sub>	0.07	0.06	3.03	3.01	0.13	305	2
3-T <sub>C</sub>	0.03	0	0.01	0	0.01	327	0
4-T <sub>HCl</sub>	0.47	14.19	3.98	2.75	0.23	443	357
4-T <sub>A</sub>	0.06	10.52	3.51	2.62	0.14	443	300
4-T <sub>B</sub>	0.06	0.01	2.71	2.7	0.17	293	0
4-T <sub>C</sub>	0.01	0	0	0	0.01	392	0
5-T <sub>HCl</sub>	0.2	4.89	2.01	1.57	0.16	439	243
5-T <sub>A</sub>	0.04	1.91	1.72	1.54	0.07	440	111
5-T <sub>B</sub>	0.06	0.01	1.6	1.59	0.05	290	0
5-T <sub>C</sub>	0.01	0	0	0	0	376	0

#### 4.2. Results of Adsorption Experiment

After the adsorption experiment, we referred to the calculation method of adsorbed hydrocarbon by Zhang et al. [25] and took the volatility of crude oil into account. The product of the adsorption experiment was extracted with a mixed solvent of DCM and

MeOH (93:7, *v/v*) for 72 h, and the unadsorbed hydrocarbons (adsorbate) were recovered. After weighing it, we performed a calculation using the following formula:

$$q = [m_{oil} \times (1 - K_{oil}) - m_{ext}] / m_a \quad (1)$$

$$Q = [1 - m_{ext} / (m_{oil} - m_{oil} \times K_{oil})] \times 100\% \quad (2)$$

Here,  $q$  (mg/g) is the crude oil adsorption capacity;  $m_{oil}$  (mg) is the weight of the adsorbate (crude oil);  $K_{oil}$  (%) is the volatilization ratio of the adsorbate (crude oil) during the process of the adsorption experiment, which was 14.27% (the date is the average value that measured multiple times in under the experimental conditions of continued the crude oil comparison group at 90 °C for 24 h);  $m_{ext}$  (mg) is the unadsorbed hydrocarbons that were extracted in the adsorption experiment;  $m_a$  (g) is the wight of adsorbent; and  $Q$  (wt.%) is the crude oil adsorption ratio. Then, we obtained the adsorption capacity (Equation (1)) and the crude oil adsorption ratio (Equation (2)) of different types of adsorbents (Table 3).

**Table 3.** The date of adsorption capacity and adsorption ratio.

No.	Adsorption Capacity (mg/g)	Adsorption Ratio (wt.%)
1-T <sub>A</sub>	1.14	19.02
1-T <sub>B</sub>	1.96	32.76
1-T <sub>C</sub>	0.97	16.23
2-T <sub>A</sub>	1.32	22.34
2-T <sub>B</sub>	1.86	31.55
2-T <sub>C</sub>	1.00	17.02
3-T <sub>A</sub>	0.84	17.55
3-T <sub>B</sub>	1.27	26.48
3-T <sub>C</sub>	0.54	11.36
4-T <sub>A</sub>	2.23	22.64
4-T <sub>B</sub>	3.31	33.51
4-T <sub>C</sub>	1.15	11.67
5-T <sub>A</sub>	1.47	25.52
5-T <sub>B</sub>	2.24	38.98
5-T <sub>C</sub>	0.93	16.23

The date of the adsorption capacity and adsorption ratio (Table 3) showed that the different samples of three types of adsorbents had the same trend of adsorption ratio for crude oil, among which T<sub>B</sub> had the highest crude oil adsorption ratio and adsorption capacity per unit mass, followed by T<sub>A</sub>, and then, T<sub>C</sub>. This indicated that the evolution state of the adsorbent had a great influence on its own adsorption performance of crude oil. Meanwhile, the crude oil adsorption ratio of the same types of adsorbent were obviously different; it was evident that the difference of the samples had an influence on the adsorption properties of the same type of adsorbent. So, it was necessary to analyze the influence of kerogen and inorganic minerals on the crude oil adsorption properties.

Based on Table 3, the adsorbate content with the adsorption capacity (Figure 4a) and the adsorbents with the adsorption ratio (Figure 4b) were drawn. Upon combining Figure 4 with Figure 2, it was found that although T<sub>C</sub> contained only inorganic minerals and lost more clay minerals than T<sub>A</sub> and T<sub>B</sub>, the crude oil adsorption ratio of T<sub>C</sub> was not much lower than that of T<sub>A</sub> and T<sub>B</sub>, which implies that the more clay minerals contained in T<sub>A</sub> and T<sub>B</sub> is more important for its adsorption properties. Meanwhile, after the pyrolysis treatment, the changes in the kerogen content and structure, inorganic mineral content, and surface properties of T<sub>B</sub> were much greater than those of T<sub>A</sub>, which may be the main reason that T<sub>B</sub> had the highest crude oil adsorption capacity. Therefore, further analysis of the crude oil adsorption capacity of T<sub>B</sub> is needed.

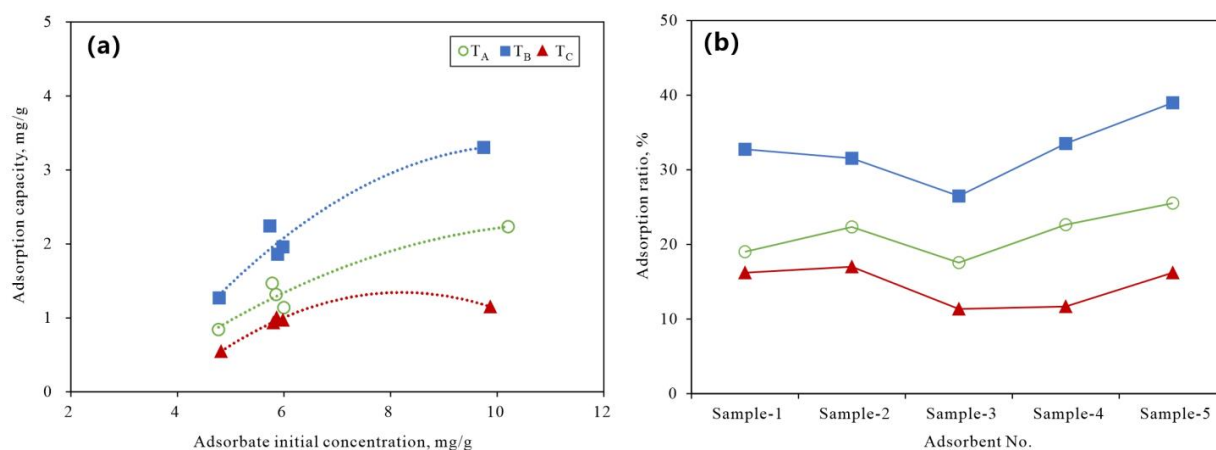


**Figure 4.** Adsorbate content with adsorption capacity (a), and adsorbents with adsorption ratio (b).

Figure 4a shows that, with an adsorbate content increase, the adsorption capacity gradually approached saturation. In this process, and with the adsorbents in an unsaturated adsorption equilibrium state, the adsorbate content (corresponding to the chloroform bitumen C content of  $T_{HCl}$ ) determined the adsorption capacity in the adsorption equilibrium stage. This result conformed to the original intention of this experiment's design: to observe the adsorption properties of the different shale adsorbents of crude oil under the condition of the content of adsorbate being close to the oil content of geological samples. Figure 4b shows that when the  $T_A$  of samples 1, 2, and 4, the  $T_B$  of samples 2 and 4, and the  $T_C$  of samples 3 and 4 had different adsorbate contents, the adsorption ratio of crude oil was basically the same, indicating that adsorbate content cannot determine the crude oil adsorption ratio of shale.

The adsorbents prepared from different shale samples had obvious differences in their crude oil adsorption ratios. For example, the different types of adsorbents in sample 3 had the lowest crude oil adsorption ratios. As shown in Figure 2, among the same types of adsorbent, sample 3 had the lowest levels of clay and feldspar mineral content. Other adsorbents with higher contents of clay and feldspar minerals generally had higher crude oil adsorption ratios, indicating that the content of inorganic minerals in shale adsorbents had a significant effect on crude oil adsorption performance in shale. However, compared with  $T_A$ ,  $T_B$  lost more clay minerals, but its crude oil adsorption ratio was higher than that of  $T_A$ . The reasons for this phenomenon also need to be analyzed.

## 5. Discussion

### 5.1. Crude Oil Adsorption Ratio of Kerogen

As  $T_C$  does not contain organic carbon, only the organic carbon content of  $T_A$  and  $T_B$  needs to be compared with the crude oil adsorption ratio. By comparing the organic carbon content of the same types of adsorbents with the crude oil adsorption ratio, it was found that there was a negative correlation between the crude oil adsorption ratio and the TOC of the adsorbents. The crude oil adsorption ratio generally increased with decreasing TOC (Figure 5a,b). This phenomenon is contrary to previous adsorption experiments using purified kerogen that showed that the kerogen content was the main controlling factor in the adsorption of crude oil, but similar to some studies that demonstrated that kerogen in shale was not the main adsorbent of hydrocarbon [26,64,65]. As can be seen from Figures 2 and 5b, the adsorbent prepared from sample 5 had the highest crude oil adsorption ratio and the highest I + S content among the same types of adsorbent. The adsorbent prepared from sample 3 had the lowest crude oil adsorption ratio and the lowest I + S content among the same types of adsorbent. Both of these results indicate that in actual shale, an increase in organic carbon (TOC = 1.60–4.52%) content cannot improve the crude oil adsorption ratio in shale and cannot dominate crude oil adsorption in shale. However, the crude oil adsorption ratio may be more affected by clay minerals.

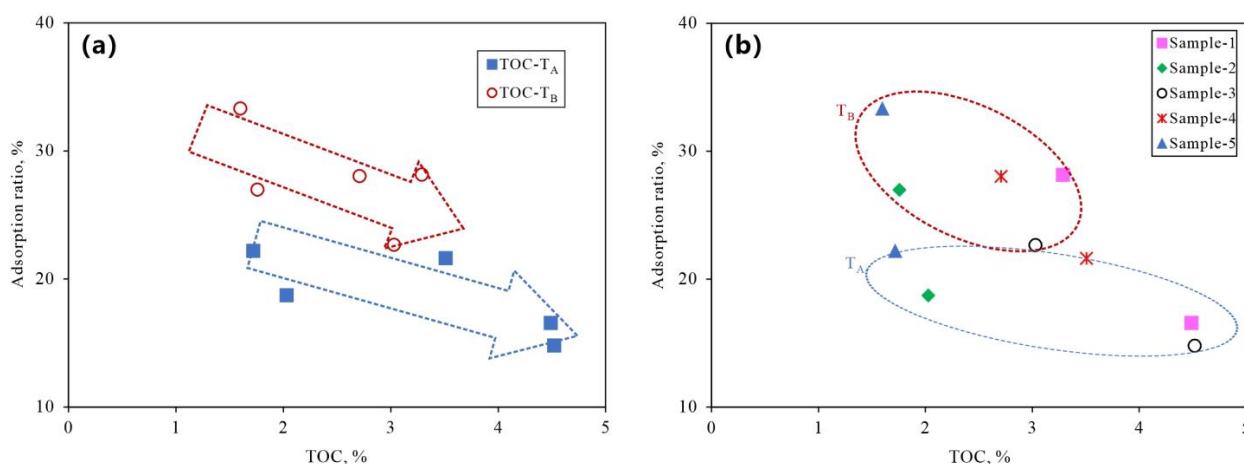


**Figure 5.** Relationship between the adsorption ratio of crude oil (a) and the TOC of adsorbents (b).

Meanwhile, only RC was retained in T<sub>B</sub> after pyrolysis (TOC  $\approx$  RC), and the TOC was decreased compared with that of T<sub>A</sub>. The ineffective carbon in kerogen in T<sub>B</sub> had a stable molecular structure and fewer side chains; however, the effective carbon in kerogen in T<sub>A</sub> was more similar to that in crude oil in terms of its molecular structure and side chains. According to the chemical principle of “like attracts like”, the crude oil adsorption properties of ineffective carbon in kerogen in T<sub>B</sub> may be lower than those of the effective carbon in kerogen in T<sub>A</sub>. However, the crude oil adsorption ratio of T<sub>B</sub> was in fact higher than that of T<sub>A</sub> (Figure 5a). Considering the conditions of preparing for T<sub>A</sub> and T<sub>B</sub>, there were obvious differences in the composition and content of inorganic minerals (Figure 2). Therefore, in determining the reasons for the increase in the crude oil adsorption ratio in T<sub>B</sub>, we need to consider the impact of inorganic minerals.

Using theoretical calculation, Tian et al. [66] considered that the oil adsorption capacity of type I and II<sub>1</sub> kerogen was 130–150 mg/g. Using adsorption experiments, Zhang et al. [25] found that the crude oil adsorption capacity of the purified kerogen in two shale samples was 123.07 mg/g and 142.29 mg/g. If the TOC (2.78% and 1.89%, respectively) of the two shale samples was taken into consideration, the crude oil adsorption capacity of kerogen in shale is calculated, respectively, to be 3.42 mg/g and 2.69 mg/g. However, the crude oil adsorption capacity on the residues of the two shale samples after ternary extraction, respectively, was 3.03 mg/g and 3.74 mg/g, among which the crude oil adsorption capacity of inorganic minerals was between 2.72 and 3.13 mg/g. The weighted sum of the crude oil adsorption capacities of kerogen and inorganic minerals were much higher than in reality. We can see that the close combination of kerogen and inorganic minerals in shale may limit the crude oil adsorption of kerogen [67], so the crude oil adsorption capacity of inorganic minerals needs further consideration.

### 5.2. Adsorption Ratio of Inorganic Minerals to Crude Oil

There was a correlation between the crude oil adsorption ratio and the relative content of the main inorganic minerals in the adsorbent (Figure 6). Among them, the relative content of different inorganic minerals in T<sub>A</sub> and T<sub>B</sub> had a positive correlation with the adsorption ratio of crude oil, but had a negative correlation with the relative content of quartz (Figure 6a,c,e). The correlation between the relative content of different inorganic minerals in T<sub>A</sub> and the adsorption ratio of crude oil was poor, which suggests that the type of inorganic minerals was not the only factor affecting the adsorption capacity of shale adsorbents for crude oil, which may also be related to the evolution state of shale. In the adsorbent prepared from the same shale sample, the change in the content of different inorganic minerals also had an obvious response to the crude oil adsorption ratio of shale (Figure 6b,d,f). When the relative content of clay minerals and feldspar decreased, the crude oil adsorption ratio also generally decreased, but the change in relative quartz content

and the crude oil adsorption ratio was the opposite. It follows that the differences in the composition and evolution state of inorganic minerals in different shale samples may have been the main reason for the differences in the crude oil adsorption properties of the same type of adsorbent.

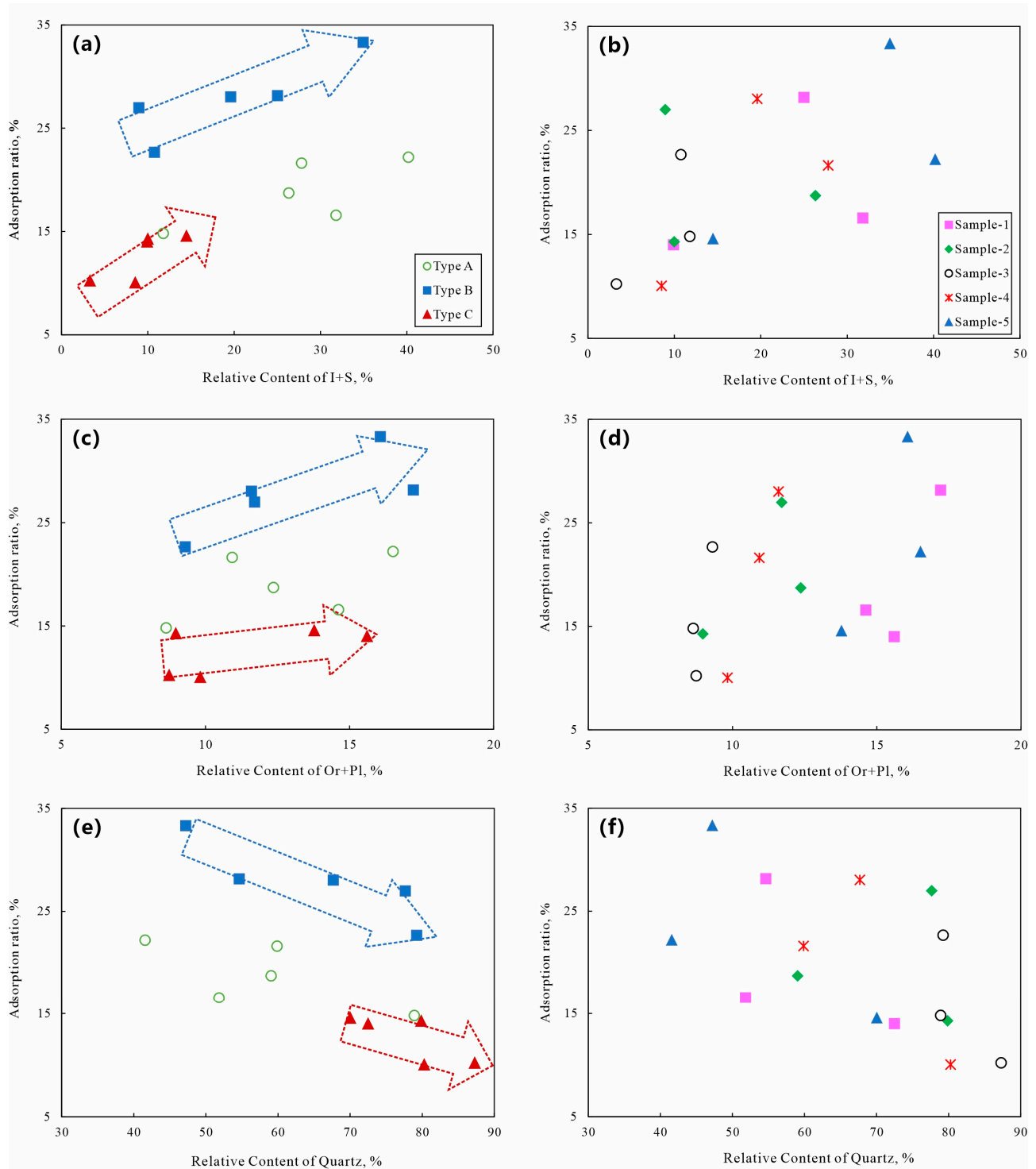


**Figure 6.** Relationship between the adsorption ratio of crude oil and the relative content of minerals. The adsorption ratio of crude oil and relative content of I + S (a), Or + Pl (c), Quartz (e) of three types of adsorbent ( $T_A$ ,  $T_B$ , and  $T_C$ ); The adsorption ratio of crude oil and relative content of I + S (b), Or + Pl (d), Quartz (f) of five types of shale adsorbent (Sample-1, Sample-2, Sample-3, Sample-4, Sample-5).

Therefore, it is necessary to analyze the ability of inorganic minerals to adsorb liquid hydrocarbon. Daughney [28] experimentally demonstrated that the maximum crude oil adsorption capacity of powdered quartz was close to 2 mg/g. Clay minerals have a wide crude oil adsorption range due to their complex structure and surface properties [68,69]; for example, Pernyeszi et al. [17] indicated that the amount of bitumen adsorbed on kaolin and illite was 33.9 mg/g and 17.1 mg/g, respectively. Li et al. [21] indicated that the maximum crude oil adsorption capacity of purified clay and quartz was 18.0 mg/g and 3.0 mg/g, respectively. In this experiment, more than 40% of the minerals in T<sub>A</sub> were quartz, and about 10–40% were clay minerals. Compared with T<sub>A</sub>, the content of clay minerals in T<sub>B</sub> decreased and the content of quartz increased slightly. The average mineral composition of T<sub>C</sub> was more than 70% quartz and about 10% clay minerals (Figure 3). According to this, we estimated that the crude oil adsorption capacity of inorganic minerals in T<sub>A</sub> and T<sub>B</sub> should be between the adsorption capacity of quartz and clay minerals, and the adsorption capacity of inorganic minerals in T<sub>C</sub> should be slightly higher than the adsorption capacity of quartz, which is close to the experimental values.

However, the crude oil adsorption capacity of inorganic minerals in the actual shale is not equal to the weighted sum of the adsorption capacity of all inorganic minerals. The change in the pore characteristics of shale also need to be considered because of the evolution of inorganic minerals. For example, the content of I + S in T<sub>B</sub> is less than that in T<sub>A</sub>, and according to the weighted sum of the mineral crude oil adsorption capacity, the crude oil adsorption ratio of T<sub>A</sub> is higher than that of T<sub>B</sub>. However, the crude oil adsorption capacity of T<sub>B</sub> is in fact significantly higher than that of T<sub>A</sub> and T<sub>C</sub>. Therefore, it is necessary to further discuss the mechanism of shale's adsorption of crude oil.

### 5.3. Discussion of the Adsorption Mechanism

Previous adsorption experiments have shown that the specific surface area (SSA) of adsorbents significantly affected their adsorption properties [70,71]. Moreover, based on the theoretical adsorption model, the SSA of the adsorbent is calculated using the amount of gas adsorption. Many scholars have studied the SSA of common minerals (Table 4), and the statistical results showed that for smectite > illite/smectite > illite > feldspar > quartz, the SSA of feldspar was slightly higher than that of quartz and much lower than that of clay minerals; this sequence is consistent with the sequence of the adsorption properties of inorganic minerals to hydrocarbons [17,19,21,29,72–76].

**Table 4.** Specific surface area (SSA) of common minerals in petroliferous basins.

Almon et al. (1981) [72]		Zhao et al. (1995) [74]		Zhang et al. (2020) [75]	
Minerals	Specific Surface Area (SSA) (m <sup>2</sup> /g)	Minerals	Specific Surface Area (SSA) (m <sup>2</sup> /g)	Minerals	Specific Surface Area (SSA) (m <sup>2</sup> /g)
smectite	820	smectite	470	orthoclase	5.745
illite	113	illite-smectite	220~297	plagioclase	3.380
chlorite	42	illite	78.66		
kaolinite	23	chlorite	65		
quartz	0.15	kaolinite	32		

Figure 7 shows a compilation of data from other authors collected by Li et al. (2016), which demonstrates a positive relationship between the specific surface area and the adsorption capacity of minerals in reservoir [21]. Meanwhile, conditions of 300–650 °C during the preparation of T<sub>A</sub> and T<sub>B</sub>, accompanied by organic hydrocarbon generation and inorganic mineral transformation (especially the transformation of I + S) [52–54,63], led to a decrease in the relative content of I + S in T<sub>B</sub>; however, with the formation of organic and inorganic pores, the SSA of shale adsorbents gradually increased [22,77,78]. This also resulted in the adsorption properties of T<sub>B</sub> being higher than those of T<sub>A</sub>. When prepared for T<sub>C</sub> (900 °C), the SSA of the adsorbents were greatly reduced due to the high degree of the dehydrox-

ylation reaction and the amorphous transformation (sintering phenomenon) of illite and other minerals [61,79,80]; this resulted in the adsorption properties of  $T_C$  being higher than those of  $T_B$ . Some collected data show that the SSA changes during the pyrolysis of shale samples (before carbonate decomposition) and during the high-temperature calcination of clay minerals (Figure 8) were consistent with the above argument [42,80]. Therefore, the relative content of clay minerals in  $T_B$  is reduced because of the transformation, but more inorganic pores are generated, which leads to the SSA of  $T_B$  being higher than that of  $T_C$  and  $T_A$ . This should be the main reason that the content of clay minerals in  $T_B$  is decreased while the crude oil adsorption ratio is highest.

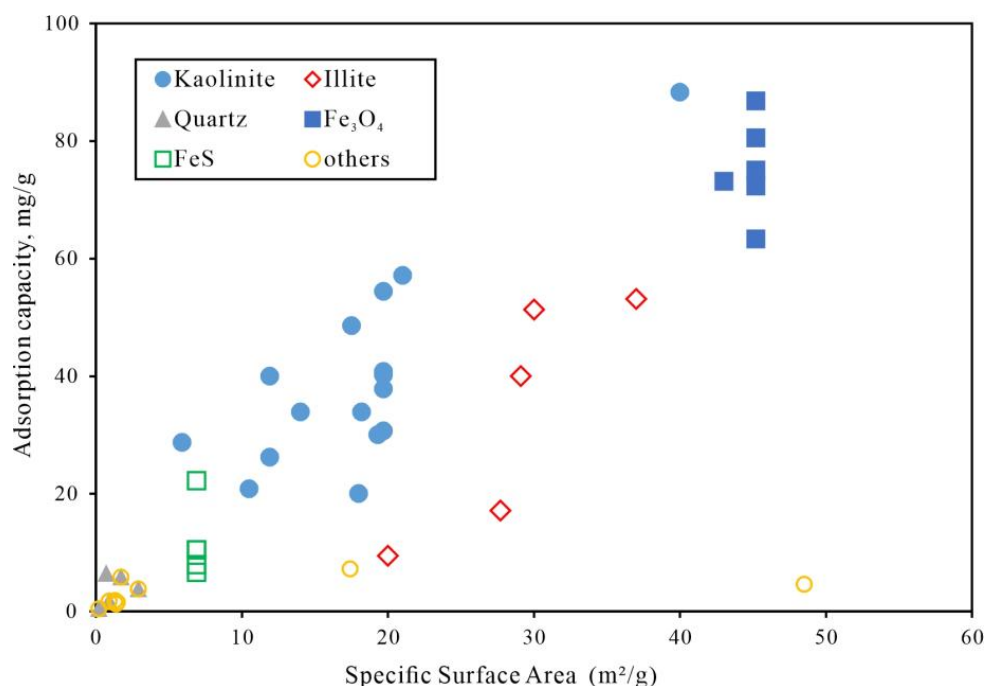


**Figure 7.** Diagram of specific surface area and adsorption capacity of minerals and reservoir rocks (Adapted with permission from Ref. [21]. 2016, Elsevier).

Meanwhile, the statistical results of the relative contents of feldspar (Pl + Or) in adsorbents varied slightly (Figures 2 and 3), so the crude oil adsorption properties of feldspar minerals were small and stable. However, the  $K^+$  provided by the dissolution of orthoclase will promote the transformation of illite/smectite to illite, and the inorganic pores formed in this process will change the SSA of the adsorbent to a certain extent; so, the existence of orthoclase will indirectly affect the crude oil adsorption properties of shale by affecting the transformation of illite/smectite to illite.

In conclusion, it was seen that the contribution of kerogen to the overall adsorption properties of shale was smaller. Meanwhile, the relative content of kerogen in the adsorbents was increased because of the removal of carbonate minerals via hydrochloric acid treatment, which meant that the relative content of kerogen in the actual shale sample was lower, and the impact of kerogen on shales to adsorption of crude oil was further reduced. Combining these two factors and the above analysis, we can conclude that in the selected general organic-rich shale (TOC = 1.60–4.52%), because the relative content of inorganic minerals is much higher than that of kerogen, and the combination of kerogen with inorganic minerals limits the contact between kerogen and crude oil, the change in kerogen's structural unit and content cannot dominate the crude oil adsorption of actual shale. On the contrary, the composition and evolution of inorganic minerals dominate the crude oil adsorption of actual shale samples.

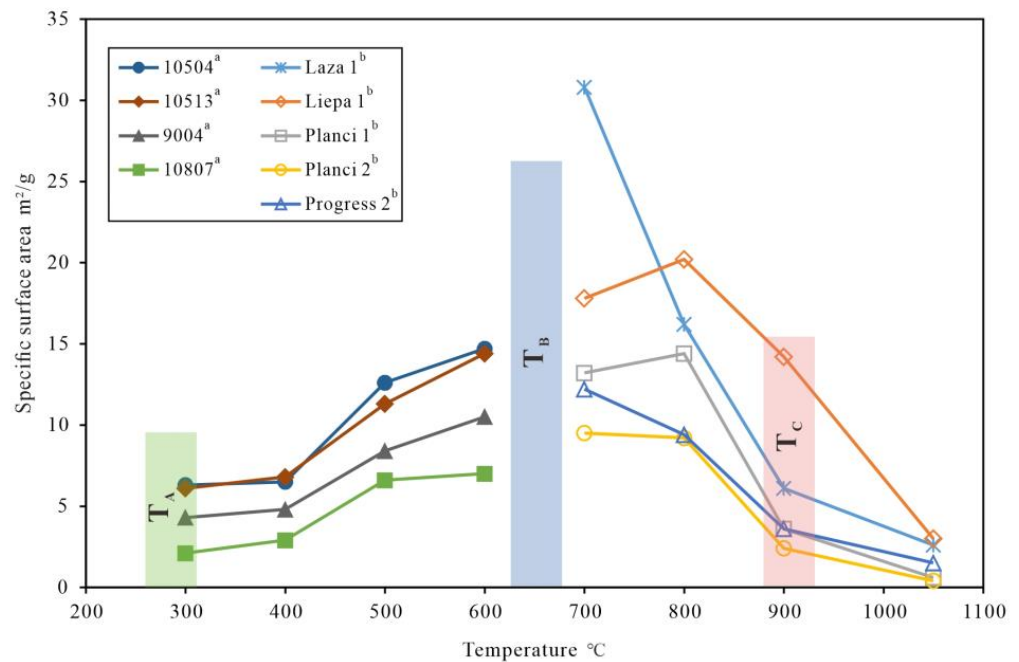


**Figure 8.** Effect of temperature on the specific surface area of shale samples and clay minerals. Left: Four groups of data on shale samples, referenced and adapted with permission from Ref. [42], marked with “a”. These shale samples were not treated with hydrochloric acid, and the carbonate minerals were largely decomposed when the temperature was higher than 600 °C, which increased the SSA of the shale samples. Therefore, only data for temperatures lower than 600 °C can represent the pyrolysis characteristics of  $T_A$  and  $T_B$  in this experiment. Right: Five groups of data on clay minerals, referenced from Dabare and Svinka [80], marked with “b”. The changes in SSA in several clay minerals (calcination at 700–1050 °C) were not affected by the thermal decomposition of carbonate. Moreover, the composition of the main inorganic minerals was basically consistent with that of  $T_{HCl}$ , so this study can approximately reflect the changes in the SSA of  $T_C$  in this experiment.

## 6. Conclusions

- (1) Under the condition of the adsorbate content being close to the oil content of geological shale samples, the crude oil adsorption capacity of  $T_A$  (containing kerogen effective carbon) ranged from 1.39 to 3.66 mg/g, and the adsorption ratio ranged from 17.56 to 25.52%. The crude oil adsorption capacity of  $T_B$  (containing kerogen ineffective carbon) ranged from 1.77 to 4.12 mg/g, and the adsorption ratio ranged from 26.48 to 38.98%. The crude oil adsorption capacity of  $T_C$  (only inorganic minerals) ranged from 1.18 to 2.40 mg/g, and the adsorption ratio ranged from 11.36 to 17.02%. The change in the surface properties of shale adsorbents during thermal evolution was the main reason for the different crude oil adsorption properties of different types of adsorbent.
- (2) In the adsorbents prepared from general organic-rich shale samples (TOC = 1.60–4.52%), because of the wide content difference between kerogen and inorganic minerals, resulting in a change in kerogen’s structural units and content, it cannot dominate the crude oil adsorption of shale. On the contrary, the composition and evolution of inorganic minerals are closely related to the crude oil adsorption properties of shale, and they play a dominant role in shale’s adsorption of crude oil. Among them, the content and evolution characteristics of illite + smectite in shale had the most significant effect on the adsorption of crude oil, and orthoclase can indirectly affect the crude oil adsorption properties of shale by affecting the conversion process of illite/smectite to illite.

**Author Contributions:** Conceptualization, S.L.; methodology, S.L. and Y.Z.; validation, Y.Z.; investigation, S.L., Y.Z. and C.Z.; resources, S.L.; data curation, Y.Z.; writing—original draft preparation, Y.Z.; writing—review and editing, S.L. and S.H.; supervision, S.L. and C.Z.; project administration, S.L. All authors have read and agreed to the published version of the manuscript.

**Funding:** This research was funded by the National Natural Science Foundation of China, grant number 42073067.

**Data Availability Statement:** Not applicable.

**Acknowledgments:** This research was financially supported by the National Natural Science Foundation of China (grant no. 42073067). We sincerely appreciate all anonymous reviewers and the handling editor for their comments and suggestions.

**Conflicts of Interest:** The authors declare no conflict of interest.

## References

1. Jarvie, D.M. Shale Resource Systems for Oil and Gas: Part2-Shale-Oil Resource Systems. *Shale Reserv.-Giant Resour. 21st Century* **2012**, *97*, 89–119.
2. Zou, C.N.; Yang, Z.; Cui, J.W.; Zhu, R.K.; Hou, L.H.; Tao, S.Z.; Yuan, X.J.; Wu, S.T.; Lin, S.H.; Wang, L.; et al. Formation mechanism, geological characteristics and development strategy of nonmarine shale oil in China. *Pet. Explor. Dev.* **2013**, *40*, 15–27. [[CrossRef](#)]
3. Modica, C.J.; Lapiere, S.G. Estimation of kerogen porosity in source rocks as a function of thermal transformation: Example from the Mowry Shale in the Powder River Basin of Wyoming. *AAPG Bull.* **2012**, *96*, 87–108. [[CrossRef](#)]
4. Jiang, Q.G.; Li, M.W.; Qian, M.H.; Li, Z.M.; Li, Z.; Huang, Z.K.; Zhang, C.M.; Ma, Y.Y. Quantitative characterization of shale oil in different occurrence states and its application. *Pet. Geol. Exp.* **2016**, *38*, 842–849.
5. Li, S.F.; Hu, S.Z.; Xie, X.N.; Lv, Q.; Huang, X.; Ye, J.R. Assessment of shale oil potential using a new free hydrocarbon index. *Int. J. Coal Geol.* **2016**, *156*, 74–85. [[CrossRef](#)]
6. Lafargue, E.; Marquis, F.; Pillot, D. Rock-Eval 6 applications in hydrocarbon exploration, production, and soil contamination studies. *Rev. L'institut Français Pétrole* **1998**, *53*, 421–437. [[CrossRef](#)]
7. Ritter, U. Fractionation of petroleum during expulsion from kerogen. *J. Geochem. Explor.* **2003**, *78–79*, 417–420. [[CrossRef](#)]
8. Ertas, D.; Kelemen, S.R.; Halsey, T.C. Petroleum Expulsion Part 1. Theory of Kerogen Swelling in Multicomponent Solvents. *Energy Fuels* **2006**, *20*, 295–300. [[CrossRef](#)]
9. Kelemen, S.R.; Walters, C.C.; Ertas, D.; Kwiatek, L.M.; Curry, D.J. Petroleum Expulsion Part 2. Organic Matter Type and Maturity Effects on Kerogen Swelling by Solvents and Thermodynamic Parameters for Kerogen from Regular Solution Theory. *Energy Fuels* **2006**, *20*, 301–308. [[CrossRef](#)]
10. Pepper, A.S.; Corvi, P.J. Simple Kinetic-Models of Petroleum Formation.1. Oil and Gas Generation from Kerogen. *Mar. Pet. Geol.* **1995**, *12*, 291–319. [[CrossRef](#)]
11. Pepper, A.S.; Corvi, P.J. Simple kinetic models of petroleum formation. Part III: Modelling an open system. *Mar. Pet. Geol.* **1995**, *12*, 417–452. [[CrossRef](#)]
12. Jarvie, D.M. Components and processes affecting producibility and commerciality of shale resource systems. *Geol. Acta* **2014**, *12*, 307–325.
13. Jarvie, D.M.; Hill, R.J.; Ruble, T.E.; Pollastro, R.M. Unconventional shale-gas systems: The Mississippian Barnett Shale of north-central Texas as one model for thermogenic shale-gas assessment. *AAPG Bull.* **2007**, *91*, 475–499. [[CrossRef](#)]
14. Li, Z.M.; Tao, G.L.; Li, M.W.; Jiang, Q.G.; Cao, T.T.; Liu, P.; Qian, M.H.; Xie, M.M.; Li, Z. Favorable interval for shale oil prospecting in coring Well L69 in the Paleogene Es3L in Zhanhua Sag, Jiyang Depression, Bohai Bay Basin. *Oil Gas Geol.* **2019**, *40*, 236–247.
15. Cai, Y.L.; Zhang, X.; Zou, Y.R. Solvent swelling: A new technique for oil primary migration. *Geochimica* **2007**, *36*, 351–356.
16. Collins, S.H.; Melrose, J.C. Adsorption of Asphaltenes and Water on Reservoir Rock Minerals. *SPE Oilfield Geotherm. Chem. Symp.* **1983**, 249–254. [[CrossRef](#)]
17. Perneszi, T.; Patzko, A.; Berkesi, O.; Dekany, I. Asphaltene adsorption on clays and crude oil reservoir rocks. *Colloids Surf. A Physicochem. Eng. Asp.* **1998**, *137*, 373–384. [[CrossRef](#)]
18. Schettler, P.D., Jr.; Parmely, C.R. Contributions to Total Storage Capacity in Devonian Shales. In Proceedings of the SPE Eastern Regional Meeting, Lexington, KY, USA, 23 October 1991.
19. Cao, Z.; Jiang, H.; Zeng, J.H.; Hakim, S.; Lu, T.Z.; Xie, X.M.; Zhang, Y.C.; Zhou, G.G.; Wu, K.Y.; Guo, J.R. Nanoscale liquid hydrocarbon adsorption on clay minerals: A molecular dynamics simulation of shale oils. *Chem. Eng. J.* **2021**, *420*, 127578. [[CrossRef](#)]
20. Acevedo, S.; Ranaudo, M.A.; Escobar, G.; Gutiérrez, L.; Ortega, P. Adsorption of asphaltenes and resins on organic and inorganic substrates and their correlation with precipitation problems in production well tubing. *Fuel* **1995**, *74*, 595–598. [[CrossRef](#)]
21. Li, Z.; Zou, Y.R.; Xu, X.Y.; Sun, J.N.; Li, M.W.; Peng, P.A. Adsorption of mudstone source rock for shale oil—Experiments, model and a case study. *Org. Geochem.* **2016**, *92*, 55–62. [[CrossRef](#)]

22. Guo, S.B.; Mao, W.J. Division of diagenesis and pore evolution of a Permian Shanxi shale in the Ordos Basin, China. *J. Pet. Sci. Eng.* **2019**, *182*, 106351. [[CrossRef](#)]
23. Mastalerz, M.; Schimmelmann, A.; Drobniak, A.; Chen, Y. Porosity of Devonian and Mississippian New Albany Shale across a maturation gradient: Insights from organic petrology, gas adsorption, and mercury intrusion. *AAPG Bull.* **2013**, *97*, 1621–1643. [[CrossRef](#)]
24. Li, F.L.; Wang, M.Z.; Liu, S.B.; Hao, Y.W. Pore characteristics and influencing factors of different types of shales. *Mar. Pet. Geol.* **2019**, *102*, 391–401. [[CrossRef](#)]
25. Zhang, L.Y.; Bao, S.Y.; Li, J.Y.; Li, Z.; Zhu, R.F.; Zhang, L.; Wang, Y.R. Hydrocarbon and crude oil adsorption abilities of minerals and kerogens in lacustrine shales. *Pet. Geol. Exp.* **2015**, *37*, 776–780.
26. Fan, E.P.; Tang, S.H.; Zhang, C.L.; Guo, Q.L.; Sun, C.H. Methane sorption capacity of organics and clays in high-over matured shale-gas systems. *Energy Explor. Exploit.* **2014**, *32*, 927–942. [[CrossRef](#)]
27. Tian, S.S.; Xue, H.T.; Lu, S.F.; Zeng, F.; Xue, Q.Z.; Chen, G.H.; Wu, C.Z.; Zhang, S.S. Molecular Simulation of Oil Mixture Adsorption Character in Shale System. *J. Nanosci. Nanotechnol.* **2017**, *17*, 6198–6209. [[CrossRef](#)]
28. Daughney, C.J. Sorption of crude oil from a non-aqueous phase onto silica: The influence of aqueous pH and wetting sequence. *Org. Geochem.* **2000**, *31*, 147–158. [[CrossRef](#)]
29. Dudášová, D.; Simon, S.; Hemmingsen, P.V.; Sjöblom, J. Study of asphaltenes adsorption onto different minerals and clays. *Colloids Surf. A Physicochem. Eng. Asp.* **2008**, *317*, 62–72. [[CrossRef](#)]
30. Wei, Z.F.; Zou, Y.R.; Cai, Y.L.; Wang, L.; Luo, X.R.; Peng, P.A. Kinetics of oil group-type generation and expulsion: An integrated application to Dongying Depression, Bohai Bay Basin, China. *Org. Geochem.* **2012**, *52*, 1–12. [[CrossRef](#)]
31. Chen, J.H.; Philp, R.P. Porphyrin distributions in crude oils from the Jiangnan and Biyang basins, China. *Chem. Geol.* **1991**, *91*, 139–151. [[CrossRef](#)]
32. Dong, Y.L.; Zhu, X.M.; Xian, B.Z.; Hu, T.H.; Geng, X.J.; Liao, J.J.; Luo, Q. Seismic geomorphology study of the Paleogene Hetaoyuan Formation, central-south Biyang Sag, Nanxiang Basin, China. *Mar. Pet. Geol.* **2015**, *64*, 104–124. [[CrossRef](#)]
33. Song, Y.; Li, S.F.; Hu, S.Z. Warm-humid paleoclimate control of salinized lacustrine organic-rich shale deposition in the Oligocene Hetaoyuan Formation of the Biyang Depression, East China. *Int. J. Coal Geol.* **2018**, *202*, 69–84. [[CrossRef](#)]
34. Qing, J.Z. *Source Rocks in China*; Science Press: Beijing, China, 2005.
35. Sun, J.N. Evaluation of Movable Oil and Retention Mechanisms of Dongying Depression Shales. Ph.D. Thesis, University of Chinese Academy of Sciences, Guangzhou, China, 2021.
36. Sert, M.; Ballice, L.; Yüksel, M.; Saglam, M.; Reimert, R.; Erdem, S. Effect of solvent swelling on pyrolysis of kerogen (type-I) isolated from Göynük oil shale (Turkey). *J. Anal. Appl. Pyrolysis* **2009**, *84*, 31–38. [[CrossRef](#)]
37. Cooles, G.P. Calculation of petroleum masses generated and expelled from source rocks. *Org. Geochem.* **1986**, *10*, 235–245. [[CrossRef](#)]
38. Dow, W.G. Kerogen studies and geological interpretations. *J. Geochem. Explor.* **1977**, *7*, 79–99. [[CrossRef](#)]
39. Qiu, L.W.; Jiang, Z.X.; Cao, Y.C.; Qiu, R.H.; Chen, W.X.; Tu, Y.F. Alkaline diagenesis and its influence on a reservoir in the Biyang depression. *Sci. China (Earth Sci.)* **2002**, *45*, 643–653. [[CrossRef](#)]
40. Wang, Q.; Xu, F.; Bai, J.R.; Sun, B.Z.; Li, S.H.; Sun, J. Study on the Basic Physicochemical Characteristics of the Huadi an Oil Shales. *J. Jilin Univ. (Earth Sci. Ed.)* **2006**, *36*, 1006–1011.
41. Dembicki, J.H. The effects of the mineral matrix on the determination of kinetic parameters using modified Rock Eval pyrolysis. *Org. Geochem.* **1992**, *18*, 531–539. [[CrossRef](#)]
42. Bai, J.R.; Song, K.T.; Chen, J.B. The migration of heavy metal elements during pyrolysis of oil shale in Mongolia. *Fuel* **2018**, *225*, 381–387. [[CrossRef](#)]
43. Yu, Z.; Ding, K.; Han, C.; Wu, Y.; Guan, F. Adsorption of diesel oil onto natural mud shale: From experimental investigation to thermodynamic and kinetic modelling. *Int. J. Environ. Anal. Chem.* **2021**, *8*, 1–15. [[CrossRef](#)]
44. Hao, Y.M.; Lu, M.J.; Dong, C.S.; Jia, J.P.; Su, Y.L.; Sheng, G.L. Experimental Investigation on Oil Enhancement Mechanism of Hot Water Injection in tight reservoirs. *Open Phys.* **2016**, *14*, 703–713.
45. Shakeel, M.; Pourafshary, P.; Hashmet, M.R. Hybrid Engineered Water-Polymer Flooding in Carbonates: A Review of Mechanisms and Case Studies. *Appl. Sci.* **2020**, *10*, 6087. [[CrossRef](#)]
46. Zhang, J.; Lu, S.F.; Li, J.Q.; Zhang, P.F.; Xue, H.T.; Zhao, X.; Xie, L.J. Adsorption Properties of Hydrocarbons (n-Decane, Methyl Cyclohexane and Toluene) on Clay Minerals: An Experimental Study. *Energies* **2017**, *10*, 1586. [[CrossRef](#)]
47. Zeng, T.Z.; Kim, K.T.; Werth, C.J.; Katz, L.E.; Mohanty, K.K. Surfactant Adsorption on Shale Samples: Experiments and an Additive Model. *Energy Fuels* **2020**, *34*, 5436–5443. [[CrossRef](#)]
48. Rajak, V.K.; Kumar, H.; Mandal, A. Kinetics, equilibrium and thermodynamic studies of adsorption of oil from oil-in-water emulsion by activated charcoal. *Int. J. Surf. Sci. Eng.* **2016**, *10*, 600–621. [[CrossRef](#)]
49. Acar, E.T.; Ortoboy, S.; Atun, G. Adsorptive removal of thiazine dyes from aqueous solutions by oil shale and its oil processing residues: Characterization, equilibrium, kinetics and modeling studies. *Chem. Eng. J.* **2015**, *276*, 340–348. [[CrossRef](#)]
50. Zhang, H.X.; Wang, X.Y.; Liang, H.H.; Tan, T.S.; Wu, W.S. Adsorption behavior of Th(IV) onto illite: Effect of contact time, pH value, ionic strength, humic acid and temperature. *Appl. Clay Sci.* **2016**, *127*, 35–43.

51. Li, S.G.; Bai, Y.; Lin, H.F.; Yan, M.; Liu, J.B. Experimental study on the effect of temperature on the kinetics characteristics of gas adsorption on coal. *J. Xi'an Univ. Sci. Technol.* **2018**, *38*, 181–186+272.
52. Berger, G.; Lachapagne, J.C.; Velde, B.; Beaufort, D.; Lanson, B. Kinetic constrains on illitization reactions and effects of organic diagenesis in sandstone/shale sequences. *Appl. Geochem.* **1997**, *12*, 23–35. [[CrossRef](#)]
53. Velde, B.; Vasseur, G. Estimation of the diagenetic smectite to illite transformation in time-temperature space. *Am. Mineral.* **1992**, *77*, 967–976.
54. Boles, J.R.; Franks, S.J. Clay diagenesis in Wilcox sandstones of Southwest Texas; implications of smectite diagenesis on sandstone cementation. *J. Sediment. Res.* **1979**, *49*, 55–70.
55. Huang, S.J.; Huang, K.K.; Feng, W.L.; Tong, H.P.; Liu, L.H.; Zhang, X.H. Mass exchanges among feldspar, kaolinite and illite and their influences on secondary porosity formation in clastic diagenesis—A case study on the Upper Paleozoic, Ordos Basin and Xujiahe Formation, Western Sichuan Depression. *Geochimica* **2009**, *38*, 498–506.
56. Aagaard, P.; Egeberg, P.K.; Saigal, G.C.; Morad, S.Y.; Bjorlykke, K. Diagenetic albitization of detrital K-feldspars in Jurassic, Lower Cretaceous and Tertiary clastic reservoir rocks from offshore Norway; II, Formation water chemistry and kinetic considerations. *J. Sediment. Res.* **1990**, *60*, 575–581. [[CrossRef](#)]
57. Wei, W.W.; Huang, S.J.; Huan, J.L. Thermodynamic Calculation of Illite Formation and Its Significance on Research of Sandstone Diagenesis. *Geol. Sci. Technol. Inf.* **2011**, *30*, 20–25.
58. Hollanders, S.; Adriaens, R.; Skibsted, J.; Cizer, Ö.; Elsen, J. Pozzolanic reactivity of pure calcined clays. *Appl. Clay Sci.* **2016**, *132–133*, 552–560. [[CrossRef](#)]
59. Fernandez, R.; Martirena, F.; Scrivener, K.L. The origin of the pozzolanic activity of calcined clay minerals: A comparison between kaolinite, illite and montmorillonite. *Cem. Concr. Res.* **2011**, *41*, 113–122. [[CrossRef](#)]
60. He, C.L.; Osbaeck, B.; Makovicky, E. Pozzolanic reactions of six principal clay minerals: Activation, reactivity assessments and technological effects. *Cem. Concr. Res.* **1995**, *25*, 1691–1702. [[CrossRef](#)]
61. Li, G.H.; Jiang, T.; Fan, X.H.; Qiu, G.Z. Thermochemical Activation of Silicon in Illite and Its Removal. *Met. Mine* **2004**, *5*, 18–24.
62. Zhou, Z.J.; Chen, D.Z. The properties and evolution of illite at high temperature. *J. Mineral. Petrol.* **1999**, *19*, 20–22.
63. He, C.L.; Osbaeck, B.; Makovicky, E. Thermal stability and pozzolanic activity of calcined illite. *Appl. Clay Sci.* **1995**, *9*, 337–354. [[CrossRef](#)]
64. Zhu, X.J.; Cai, J.G.; Wang, G.L.; Song, M.S. Role of organo-clay composites in hydrocarbon generation of shale. *Int. J. Coal Geol.* **2018**, *192*, 83–90. [[CrossRef](#)]
65. Ross, D.; Bustin, R.M. The importance of shale composition and pore structure upon gas storage potential of shale gas reservoirs. *Mar. Pet. Geol.* **2009**, *26*, 916–927. [[CrossRef](#)]
66. Tian, S.S.; Xue, H.T.; Lu, S.F.; Chen, G.H. Discussion on the Mechanism of Oil and Gas Retention of Different Types of Kerogen, Symposium 57: Basin Dynamics and Unconventional Energy. In Proceedings of the 2014 China Geoscience Union Academic Conference, Beijing, China, 20–23 October 2014.
67. Rahman, H.M.; Kennedy, M.; Löhr, S.; Dewhurst, D.N. Clay-organic association as a control on hydrocarbon generation in shale. *Org. Geochem.* **2017**, *105*, 42–55. [[CrossRef](#)]
68. Tian, S.S.; Erastova, V.; Lu, S.F.; Greenwell, H.C.; Underwood, T.R.; Xue, H.T.; Zeng, F.; Chen, G.H.; Wu, C.Z.; Zhao, R.X. Understanding Model Crude Oil Component Interactions on Kaolinite Silicate and Aluminol Surfaces: Toward Improved Understanding of Shale Oil Recovery. *Energy Fuels* **2018**, *32*, 1155–1165. [[CrossRef](#)]
69. Jada, A.; Debih, H. Hydrophobation of Clay Particles by Asphaltene Adsorption. *Compos. Interfaces* **2012**, *16*, 219–235. [[CrossRef](#)]
70. Chu, X.Z.; Xu, J.M. Relationship between the Adsorption Capacity of Hydrogen Isotopes and Specific Surface Area of Adsorbents. *Chem. J. Chin. Univ.-Chin. Ed.* **2008**, *29*, 775–778.
71. Nijkamp, M.G. Hydrogen Storage using Physisorption: Modified Carbon Nanofibers and Related Materials. Ph.D. Thesis, Utrecht University Repository, Utrecht, The Netherlands, 2001.
72. Almon, W.; Davies, D.K.; Longstaffe, F. Formation damage and the crystal chemistry of clays. *Short Course Clays Resour. Geol. Montr. Mineral. Assoc. Can.* **1981**, *7*, 81–102.
73. Olphen, V.H.; Fripiar, J.J. *Data Handbook for Clay Materials and Other Non-Metallic Minerals*; Pergamon Press: Oxford, UK; Elmsford, NY, USA, 1979; Volume 131, pp. 62–63.
74. Zhao, X.Y.; Zhang, Y.Y.; Song, J. Some mineralogical characteristics of clay minerals in China oil-bearing basins. *Geoscience* **1994**, *8*, 254–272.
75. Zhang, W.; Ren, Y.N.; Zhao, X.L.; Yan, T.G.; Sun, Q. Investigations of the adsorption of fluoride on natural sodium feldspar and potassium feldspar in aqueous solution. *J. Yunnan Univ. Nat. Sci. Ed.* **2020**, *42*, 977–984.
76. Yazdani, R.; Tuutijarvi, T.; Bhatnagar, A.; Vahala, R. Adsorptive removal of arsenic(V) from aqueous phase by feldspars: Kinetics, mechanism, and thermodynamic aspects of adsorption. *J. Mol. Liq.* **2016**, *214*, 149–156. [[CrossRef](#)]
77. Wu, S.T.; Zhu, R.K.; Cui, J.G.; Cui, J.W.; Bai, B.; Zhang, X.X.; Jin, X.; Zhu, D.S.; You, J.C.; Li, X.H. Characteristics of lacustrine shale porosity evolution, Triassic Chang 7 Member, Ordos Basin, NW China. *Pet. Explor. Dev.* **2015**, *42*, 167–176. [[CrossRef](#)]
78. Liu, B.; Wang, Y.; Tian, S.S.; Guo, Y.L.; Wang, L.; Yasin, Q.; Yang, J.G. Impact of thermal maturity on the diagenesis and porosity of lacustrine oil-prone shales: Insights from natural shale samples with thermal maturation in the oil generation window. *Int. J. Coal Geol.* **2022**, *261*, 104079. [[CrossRef](#)]

- 
79. Goodman, C.; Vahedifard, F. Micro-Scale Characterization of Clay at Elevated Temperatures. *Géotechnique Lett.* **2019**, *9*, 225–230. [[CrossRef](#)]
  80. Dabare, L.; Svinka, R. Characterization of porous ceramic pellets from Latvian clays. *Chemija* **2014**, *25*, 82–88.

**Disclaimer/Publisher’s Note:** The statements, opinions and data contained in all publications are solely those of the individual author(s) and contributor(s) and not of MDPI and/or the editor(s). MDPI and/or the editor(s) disclaim responsibility for any injury to people or property resulting from any ideas, methods, instructions or products referred to in the content.